Astrometric Measurements of Three Double Star Systems Near 5h of Right Ascension

Leonid Vishnevskiy[1], Denis Levine[1], Nicholas Dunn[1,2], Khensa Musaddequr Rahman[1], Kalée Tock1
[1] Stanford Online High School, Redwood City, California; leonid59@ohs.stanford.edu
[2] Wellington College, Berkshire, UK

Abstract

We investigate three double star systems with a right ascension between 5h and 6h, imaging them using the Las Cumbres Observatory Global Telescope network. We perform astrometric measurements using AstroImageJ, obtaining position angles and separations for all of the systems that are similar to each system's most recent measurements. Historic measurements from the US Naval Observatory are plotted, and linear and quadratic regressions are performed, with the result that a quadratic regression fits slightly, but not conclusively, better for most of the systems. Based on our measurements, historic data plots, and calculations performed using data from Gaia Data Release 3, we conclude that all of the target star systems are physically related. In addition, WDS 05553+0729 DOO 95 is likely to be binary, while WDS 05033+5821 STI 2082 and WDS 05207+2442 POU 674 are unlikely to be binary.

1. Introduction

Double star systems have the potential to be binary systems, in which the stars are mutually bound by gravitational forces. However, they are also interesting if they are physically related in any other way, such as sharing an origin. Studying the nature and evolution of this relationship gives us insight into the history and dynamics of the galaxy.

The focus of our investigation was limited to double stars listed in the Washington Double Star (WDS) Catalog, adhering to a few specific constraints:

1. Magnitude (m) secondary < 13: Both stars in each pair were constrained to be brighter than magnitude 13 so that they could be distinguished using the instruments described in Sec. 2.
2. 5" ≤ separation ≤ 15": The lower bound was chosen to ensure that our instruments can resolve two separate stars. The upper bound was chosen in hopes that the measurement we obtain would be more likely to be different from previous observations, since stars that are closer together are more likely to orbit faster. While this does not account for radial separation, the correlation still holds in general.
3. Δm < 3: The stars in the pair were constrained to be close together in magnitude, so that both could be exposed properly in a single image with a single exposure time.
4. Physical: The system was constrained to be listed as "physical" according to Stelle Doppie, which means that the two component stars have similar parallaxes and proper motions.
5. 05h < Right Ascension < 13h: The right ascension of the system was constrained to be between 05h and 13h, to ensure that it is positioned near zenith during the night at the time the study was conducted; this makes the observing position optimal. Declination was not taken into account because the telescope network we used has sites available across the globe.

The targets selected for this study according to the constraints above are all near 5 hours of right ascension. Although their magnitudes make the systems too dim to be seen with the naked eye, their approximate locations can be found by star-hopping from nearby bright stars and asterisms. For example, STI 2082 is close to Capella in the Camelopardalis constellation, and POU 674 is located inTaurus. DOO 95 is in Orion, very close to Betelgeuse. The positions of all three targets shown in Fig. 1.

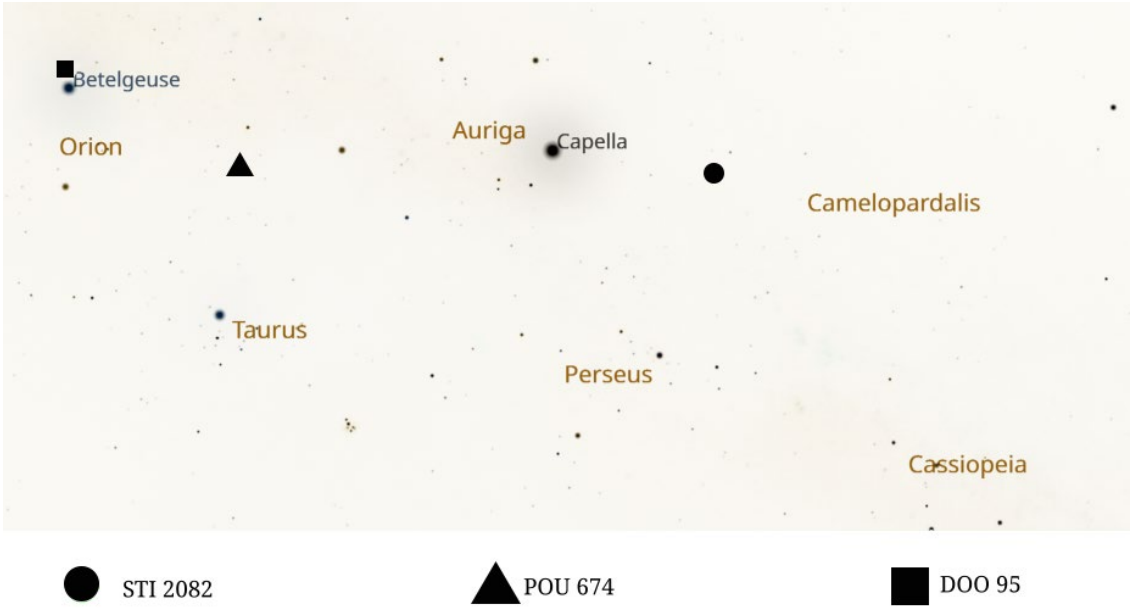

Figure 1: Approximate location of each system, relative to the surrounding constellations and bright stars

Many of these stars are Sun-like, and some are hotter than the Sun. Our measurements for each star were made eight to nine years after the last recorded data, which ranged from 2015 to 2016.

We calculated the absolute magnitude of each star using the Gaia Data Release 3 (DR3) apparent G-filter magnitude and parallax according to Eq. 1 from Morgan, 2019. We invert the distance in parsecs to get parallax, and convert the parallax from ″ to milliarcseconds:

$$mag_{abs} = mag_{vis} + 5 \times (log_{10}\,(plx \times \frac{1\,''}{1000\,mas}) + 1) \qquad \text{Eq. 1}$$

Where *plx* is the parallax of the star in milliarcseconds. Then we approximated each star's spectral class and mass using our calculations from Eq. 1 of each star's absolute magnitude, and matched this to a mass using a list relating mass to absolute magnitude (Morgan, 2023). The masses and spectral types resulting from this analysis, along with temperature values from the literature for DOO 95, are shown in Table 1.

Table 1. Masses, spectral types, and colors for each double star system.

Star System	Parallax: Primary (mas); Parallax: Secondary (mas)	Gaia DR3 Gmag (Primary; Secondary)	Gaia DR3 BP - RP (Primary; Secondary)	Spectral Type: Primary; Spectral Type: Secondary	Effective Temperature Primary; Secondary (K)	Mass: Secondary ($M_\odot$); Mass: Secondary ($M_\odot$)
WDS 05033+5821 STI 2082	1.64; 1.68	11.36; 11.57	0.46; 0.79	A5; A7	N/A	1.73; 1.61
WDS 05207+2442 POU 674	1.71; 1.73	11.76; 13.16	1.18; 1.35	A7; G0	N/A	1.61; 1.07
WDS 05553+0729 DOO 95	1.62; 1.60	12.23; 12.95	0.73; 0.83	F0; F6	6606.4; 6296.4[1]	1.44; 1.20

[1]Temperature values for DOO 95 from Wenger, 2020.

2. Equipment and Methods

We used the Las Cumbres Observatory Global Telescope (LCOGT) network to take images of all of our chosen star systems in the Bessell-V filter (Bessell, 1990). The exposure times and observatory locations used for our measurements are summarized in Table 2.

Table 2. The number of images and their exposure times for each system. All images for each system had constant exposure times.

System	Images Taken	Observatory (Location)	Exposure Time (s)
WDS 05033+5821 STI 2082	16	Teide Observatory (Tenerife, Spain)	21
WDS 05207+2442 POU 674	10	McDonald Observatory (Texas, USA)	19
WDS 05553+0729 DOO 95	10	Siding Spring Observatory (NSW, Australia)	19

All of the telescopes involved in this study used a Planewave Delta Rho 350 + QHY600 CMOS camera system, which has a field of view of 1.9° × 1.2°. However, we used the central 30' × 30' mode, which produced images each with a size of 2400 pixels × 2400 pixels and covering the camera's central 30' × 30' field of view. The pixel size of the camera is 0.73" per pixel, in 1 × 1 binning mode. The images were directly analyzed using the AstroImageJ software.

3. Measurements

3.1. Images

All LCOGT images were processed directly in AstroImageJ using its multi-aperture measurement tool, which allows the user to find the centroid of a star within an aperture, and then calculate the position angle and separation between the two centroids. Sample measurements of each system are shown in Figure 2, along with the measurement aperture radius used. Individual measurements are tabulated in Table 7 of the Appendix.

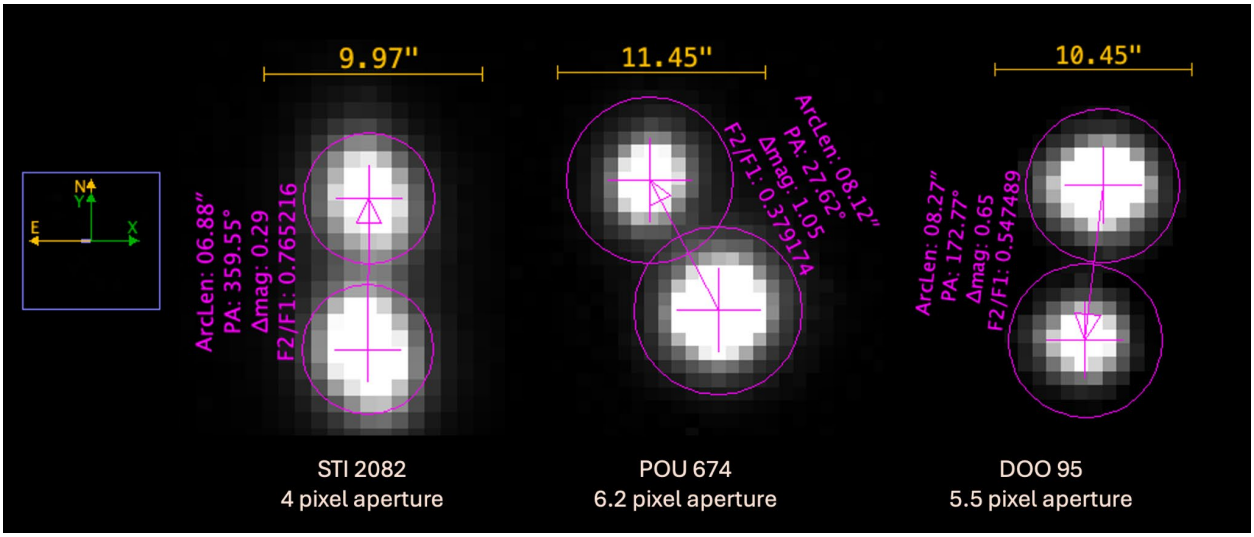

Figure 2: Measurements of STI 2082, POU 674, and DOO95 in AstroImageJ.

A summary of the measurements of the three systems is shown in Table 3, where "Number of Images Used" excludes some images that were lower in quality than those shown above.

Table 3. Summary of obtained astrometric data for all three systems.

System	Decimal Date (Epoch)	Number of Images Used	Average Position Angle (°)	Standard error on Position Angle	Average Separation (″)	Standard Error on Separation
WDS 05033+5821 STI 2082	2024.0301	14	359.5	0.05	6.93	0.019
WDS 05207+2442 POU 674	2024.0444	10	27.5	0.04	8.13	0.007
WDS 05553+0729 DOO 95	2024.0329	10	172.8	0.08	8.21	0.015

3.2 Historic Data plots

Below are historical data plots made using data from the USNO. We fit quadratic and linear fits on each system, excluding outlying points where noted, in order to assess the trends of the graphs and the plausibility of curvature. The origin represents the position of the primary star.

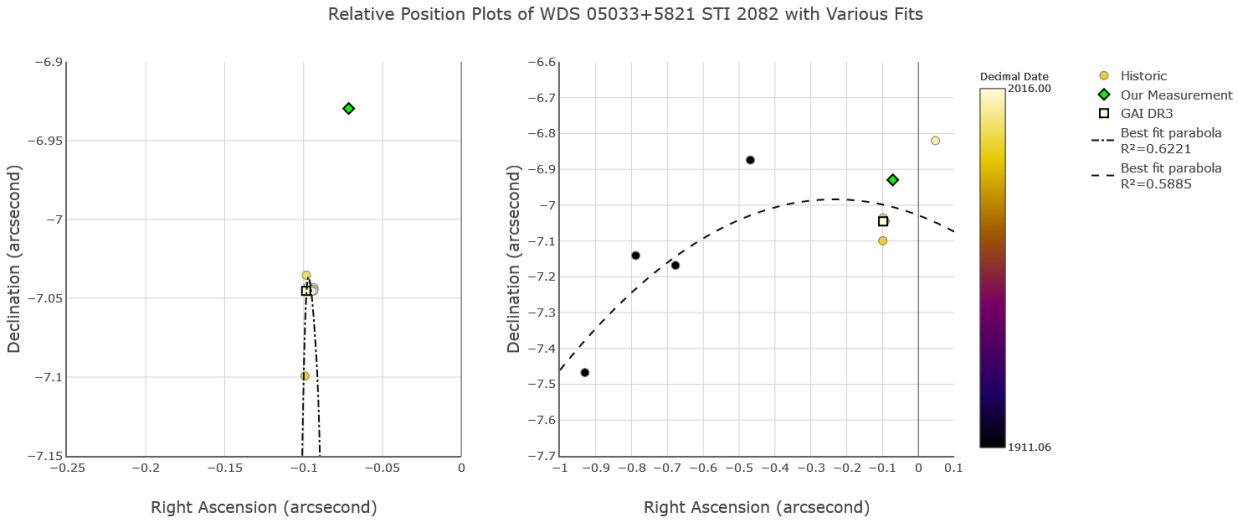

Figure 3: Relative position plots of STI 2082 with a parabolic fit. The right graph contains all points, and the left graph excludes all 1911 points and the 2010 data point

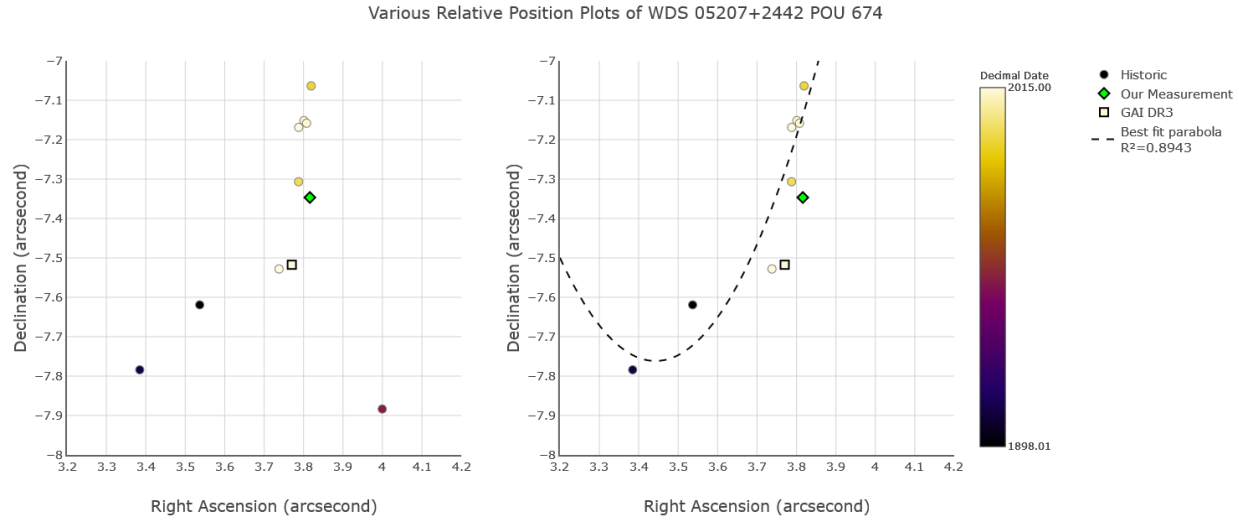

Figure 4: Relative position plot of POU 674. The left graph has all points, and the right graph excludes an outlying data point and has a parabolic fit

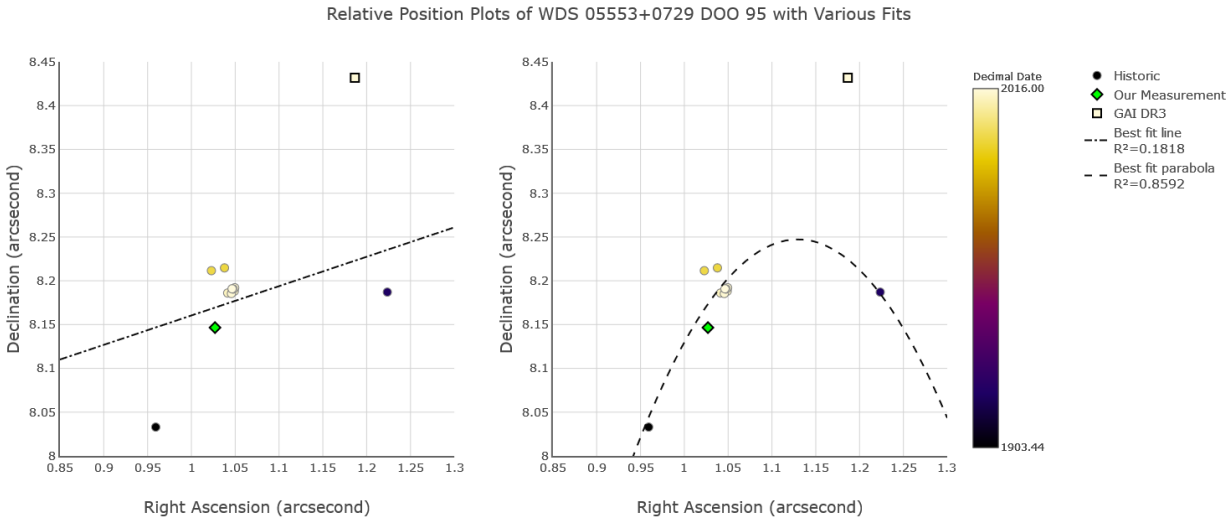

Figure 5: Relative position plots of DOO 95, excluding an outlier from Fay, 2021. The left graph has a linear fit, while the right graph has a parabolic fit.

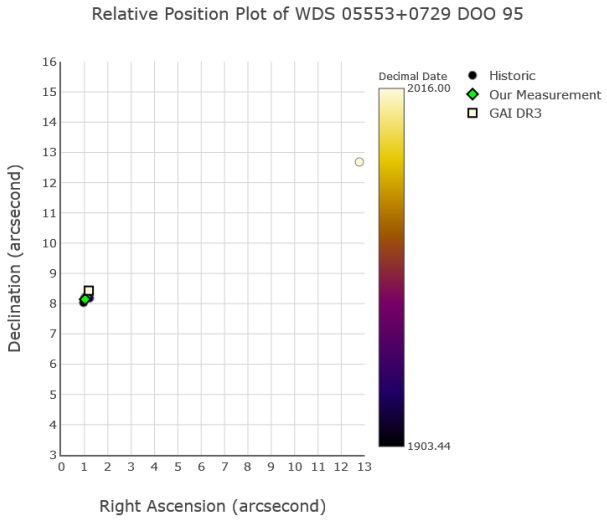

Figure 6: Relative position plot of DOO 95, with outlier included

4. Analysis of the Stars' Motions

To assess the physical relationship between the stars, we obtained proper motion and parallax data from Gaia DR3 which are shown in Table 4.

Table 4. Proper Motions and Parallaxes

System	PM RA Primary (mas/yr)	PM RA Secondary (mas/yr)	PM Dec. Primary (mas/yr)	PM Dec. Secondary (mas/yr)	Parallax of Primary (mas)	Parallax of Secondary (mas)
WDS 05033+5821 STI 2082	-0.99934 ± 0.01917	-0.96604 ± 0.01553	2.40102 ± 0.01863	2.13951 ± 0.01472	1.63893 ± 0.02424	1.68483 ± 0.01992
WDS 05207+2442 POU 674	-1.37158 ± 0.02480	-1.25725 ± 0.01866	-2.12339 ± 0.01723	-1.84413 ± 0.01285	1.71328 ± 0.02068	1.72545 ± 0.01530
WDS 05553+0729 DOO 95	4.71638 ± 0.01642	4.69297 ± 0.02168	-14.45043 ± 0.01325	-14.48876 ± 0.01826	1.61591 ± 0.01548	1.59932 ± 0.02143

We first calculate the rPM values of all the systems, which is a measure of how similar the proper motions of double star systems are and thus how likely they are to be physically related (Harshaw, 2016). A lower rPM value implies that the stars are moving together and therefore may share an origin. Next, we calculated the relative velocities of the secondary stars to the primary stars of each system as well as the escape velocity of each system; this allows us to assess the likelihood of the stars being binary.

4.1 Derivation and Calculation of rPM Values

To derive the rPM from the data, we divide the magnitude of the stars' relative motion by the magnitude of the larger proper motion vector (Harshaw, 2016). In the following equations, PM represents proper motion of the right ascension or declination, and the number suffix represents primary star (for 1) or secondary star (for 2). Pythagoras' theorem is used to combine the x and y components of the total vector. The total relative motion vector is shown in Eq. 2 below:

$$|m_r| = \sqrt{(PM\ RA\ 1\ -\ PM\ RA\ 2)^2\ +(PM\ Dec\ 1\ -\ PM\ Dec\ 2)^2} \quad \text{Eq. 2}$$

The magnitude for the proper motion vector of a singular star is computed using Eq. 3:

$$|m_{singular}| = \sqrt{(PM\ RA\ 1)^2 + (PM\ Dec\ 1)^2} \quad \text{Eq. 3}$$

We then divide the total value in Eq. 1 by the larger proper motion magnitude (out of the primary and second stars) in Eq. 2 to get the rPM for each system. This is represented in Eq. 4:

$$rPM = \frac{|m_r|}{|m_{larger}|} \quad \text{Eq. 4}$$

The results of our rPM calculations are presented in Table 5 below. According to the classification scheme defined by Harshaw (2016), all of our star systems exhibit common proper motion (CPM), meaning they share proper motion to a high degree and likely have a common origin in space.

Table 5: Results of our rPM calculations.

System	Relative PM Magnitude (mas/yr.)	Larger PM Magnitude (mas/yr)	rPM Value	Interpretation
WDS 05033+5821 STI 2082	0.2636	2.6007	0.1014	CPM
WDS 05207+2442 POU 674	0.3018	2.5279	0.1194	CPM
WDS 05553+0729 DOO 95	0.0449	15.2298	0.0030	CPM

4.2 Derivation and Calculation of Relative and Escape Velocities

To convert the relative PM vectors from angular units (mas) to physical units (meters per second), we multiply by the distance to the system, which entails dividing by the parallax of the primary star. (Since the primary and secondary of each system have similar parallax, the choice of which star's parallax to use is arbitrary.) We then multiply by several conversion factors to obtain the transverse velocity of the system:

$$V_{transverse} = PM_{Relative} \times \frac{1}{plx \times \frac{1''}{1000\ mas}} \times \frac{1\ "}{1000\ mas} \times \frac{1°}{3600\ "} \times \frac{\pi\ rad}{180\ °} \times \frac{3.086\times10^{16}\ m}{pc} \times \frac{1\ yr}{3.1536\times10^{7}\ s} \quad \text{Eq. 5}$$

Next, we need the relative radial motion through space, which is found using Eq. 6:

$$V_{radial} = 1000\ \frac{m}{km}(V_{1\ rad}\ \frac{km}{s} - V_{2\ rad}\ \frac{km}{s}) \quad \text{Eq. 6}$$

To obtain a relative 3D space velocity, we combine $V_{transverse}$ and V_{radial} using Pythagorean's Theorem.

As for the velocities, the 3D separation *r* has two components: transverse and radial. The 3D radial separation is computed from Eq. 7 using the Gaia DR3 parallaxes in Table 4. The 2D transverse separation is computed from the Washington Double Star Catalog separation using Eq. 8.

$$Sep_{radial\ 3D} = \frac{1}{\frac{plx_1\ mas}{1000\frac{mas}{arcsec}}} - \frac{1}{\frac{plx_2\ mas}{1000\frac{mas}{arcsec}}} = 1000\ \frac{mas}{arcsec}\left(\frac{1}{plx_1} - \frac{1}{plx_2}\right) \quad \text{Eq. 7}$$

$$Sep_{transverse\ 2D} = Sep_{''} \times \frac{°}{''} \times \frac{\pi}{180}\ \frac{rad}{deg} \times \frac{1}{parallax\ ''} \quad \text{Eq. 8}$$

The escape velocity can be computed according to Eq. 9, which requires the masses of the stars (m_1 and m_2) from Table 1 as well as their 3D separation in space (*r*), and the gravitational constant *G*. (Bonifacio et al., 2020).

$$V_{escape} = \sqrt{\frac{2\times G\times(m_1+m_2)}{r}} \quad \text{Eq. 9}$$

As an example, the quantities for Table 6 are calculated for STI 2082 like so. The parallaxes for the primary and secondary stares are used from Table 4, and are about 1.64 mas and 1.68 mas, respectively.

$$V_{transverse} = 0.2636 \frac{mas}{yr} \times \frac{1}{1.63893 \times \frac{1''}{1000\,mas}} \times \frac{1''}{1000\,mas} \times \frac{1°}{3600''} \times \frac{\pi\,rad}{180°} \times \frac{3.086 \times 10^{16}\,m}{pc} \times \frac{1\,yr}{3.1536 \times 10^{7}\,s}$$

$$V_{transverse} = 763\ \frac{m}{s}$$

$$V_{radial} = 1000\ \frac{m}{km}\left(-33.63518\ \frac{km}{s} + 21.25268\ \frac{km}{s}\right) = -12382.5 \frac{m}{s}$$

$$Sep_{radial} = 1000\ \frac{mas}{arcsec}\left(\frac{1}{1.63893 mas} - \frac{1}{1.68483 mas}\right) = 16.6225\ pc$$

$$Sep_{transverse} = 7.046 \times\ \frac{°}{3600''} \times \frac{\pi}{180}\ \frac{rad}{deg} \times \frac{1}{1.63893\,''} = 0.0208\text{pc}$$

$$V_{escape\ radial} = \sqrt{\frac{2 * 6.67 * 10^{-11}\ \frac{N * m^2}{kg} * 1.99 * 10^{30}\ \frac{kg}{M\odot}(1.73\,M\odot + 1.61\,M\odot)}{16.6225\,pc\ *\ 3.09\ *\ 10^{16}\ \frac{m}{pc}}} = 42\ \frac{m}{s}$$

$$V_{escape\ transverse} = \sqrt{\frac{2 * 6.67 * 10^{-11}\ \frac{N * m^2}{kg} * 1.99 * 10^{30}\ \frac{kg}{M\odot}(1.73\,M\odot + 1.61\,M\odot)}{16.6225\,pc\ *\ 3.09\ *\ 10^{16}\ \frac{m}{pc}}} = 1174\ \frac{m}{s}$$

For POU 674 and DOO 95, the parallaxes of the two component stars overlap within their respective uncertainties. Therefore, the radial separation may be taken to be 0, so that the 3D separation is equivalent to the 2D (transverse) separation. In Table 6, we show escape velocities for both cases, with the 2D separation escape velocity bolded for POU 674 and DOO 95 to indicate that, and the 3D separation escape velocity bolded for STI 2082.

Table 6. Escape velocity calculations, with the relevant escape velocity for each system bolded. Relative radial motion is listed as N/A for DOO 95 because its components' radial velocities were not listed in Gaia.

System	Relative Transverse Motion (m/s)	Relative Radial Motion (m/s)	Relative 3D Velocity (m/s)	3D Separation (pc); 2D Separation (pc)	3D Escape Velocity (m/s); 2D Escape Velocity (m/s)
WDS 05033+5821 STI 2082	763	12383	12406	16.6225; 0.0208	**42**; 1174
WDS 05207+2442 POU 674	835	4493	4570	4.1169; 0.0238	75; **985**
WDS 05553+0729 DOO 95	132	N/A	132	6.4194; 0.0243	59; **967**

For STI 2082 and POU 674 the escape velocities are much lower than the relative velocities even if the larger 3D separation is used in the calculation. Therefore, we conclude that the systems are unlikely to be gravitationally bound. However, their common proper motion implies that they are both physical systems.

For DOO 95, the case where the stars' parallax uncertainties overlap applies, so we can take the two stars to be the same distance from Earth. When considering the escape velocity of the system like this, the radial 3D velocity is much lower than the escape velocity and implies that there is a high likelihood of the system being gravitationally bound. However, in the case we take the parallaxes as directly reported by Gaia , assuming they do not overlap, the relative 3D velocity of the system is about twice that of the escape velocity, implying a low likelihood of a gravitational relationship in that case. Additionally, Gaia data does not list radial velocities for the stars in DOO 95, meaning that the relative 3D velocity of the system is likely higher than reported here. Regardless, from the data currently available, we conclude that there is a significant chance of the system being binary.

5. Discussion

5.1 STI 2082

STI 2082 and DOO 95 have a chance alignment coefficient $\mathscr{R}$ calculated by El Badry et al. (2021), which is related to the chance of a star system being an optical double and not gravitationally bound. The paper notes that this value is not directly a probability–for example, it can be higher than 1. The lower the value is, the higher chance of the system being a binary double. STI 2082 had $\mathscr{R}$ at 2.5×10^{-4}. Since the paper defines a high chance of being a binary double as a $\mathscr{R}$ value of less than 0.1, this corresponds to a 90% chance of being gravitationally bound. However, our escape velocity calculation suggests otherwise, as shown in Table 6.

STI 2082's historical data plots in Fig. 3 show weak curves that point away from the primary star, which would not indicate an orbit around the primary even if the trend were stronger. If we remove all of the points from 1911, the remaining data, with the exception of the data point from 2010, is clumped on the graph. Removing the 1911 and 2010 points results in only a few measurements. Our current measurement deviates from these, though not as strongly as the 2010 data. One hypothesis for this unexpected behavior is that the stars may have been in a position that caused their acceleration due to a mutual gravitational influence temporarily increased, but this is difficult to support with the evidence of only a few data points. In any case, this plot is inconclusive evidence of an orbital relationship between STI 2082's component stars.

5.2 Discussion of POU 674

The escape velocity versus relative velocity calculations do not support an orbital relationship for the components of POU 674, regardless of whether the 2D or 3D separation is taken as the separation between the component stars. The historical measurements also do not show evidence of a clear trend over time. The polynomial regression (excluding the potentially erroneous measurement off to the bottom left of the plot taken in 1950) does fit a curve that revolves around the origin, as would be expected for a binary system, but the trend is not sufficiently strong as to be conclusive, and a linear relationship is also possible. Based on the common proper motion of the stars, their relationship appears to be physical but not gravitational.

5.3 Discussion of DOO 95

DOO 95 has an $\mathscr{R}$ of approximately 10^{-4} , implying that it is also binary according to El Badry's criterion cited above. Even if we have overestimated the stars' masses, it is still possible that they are bound, because their relative velocity is significantly lower than the escape velocity. If the stars are not bound, we can instead say that the pair likely shares a common origin, because of the very low rPM value. Additionally, the two stars

in DOO 95 have a transverse separation of only 0.02 parsecs. Therefore, based on the available evidence, there appears to be a significant likelihood of the stars in DOO 95 being gravitationally bound to each other.

One historical measurement of DOO 95 (Fay, 2021), shown in Fig. 6, appears to be an outlier from the broader data. Using a CCD sensor on a 28.3 cm diameter camera, Fay (2021) reported a separation of 18 arcseconds and a position angle of about 135 degrees, which is substantially different than any other measurement recorded. Current models of stellar motion do not allow for such behavior, which is why we have presented an analysis of DOO 95 with and without this peculiar data point.

6. Conclusions

Both STI 2082 and POU 674 are physical doubles due to their low rPM values, but are unlikely to be gravitationally bound systems. STI 2082 has been previously listed as having a high likelihood of being binary according to El Badry's chance alignment probability coefficient value $\mathscr{R}$, but our velocity calculations imply the stars are moving too fast relative to each other to sustain a binary relationship, and the historical data plots do not imply an orbit. However, the physical similarity of the two stars and their shared motion through space imply that increased uncertainty of their positions or proper motions may lead to a different conclusion. Therefore, further measurements are recommended.

The component stars of DOO 95 are certainly physically related and have a considerable chance of the system being binary, based on our escape and relative system velocity calculations, as well as the $\mathscr{R}$ criterion of El-Badry et al. (2021). Additionally, from the historic data file from the USNO, we observed a significant increase in measurement of this system starting around 2013, which seems to stem from Gaia data. We therefore recommend further measurement of this system when considering double star system observations from telescopes or catalog data.

Acknowledgements

This research was made possible by the Washington Double Star catalog maintained by the U.S. Naval Observatory, the Stelle Doppie catalog maintained by Gianluca Sordiglioni, Astrometry.net, and AstroImageJ software which was written by Karen Collins and John Kielkopf.

This work has made use of data from the European Space Agency (ESA) mission Gaia (https://www.cosmos.esa.int/gaia), processed by the Gaia Data Processing and Analysis Consortium (DPAC, https://www.cosmos.esa.int/web/gaia/dpac/consortium). Funding for the DPAC has been provided by national institutions, in particular the institutions participating in the Gaia Multilateral Agreement.

This work makes use of observations taken by the Planewave Delta Rho 350 + QHY600 CMOS camera systems of Las Cumbres Observatory Global Telescope Network at the Siding Spring Observatory in New South Wales, Australia; Teide Observatory at Mount Teide, Spain; and the McDonald observatory in Fort Davis, Texas. The Las Cumbres Observatory's education network telescopes were upgraded through generous support from the Gordon and Betty Moore Foundation.

This research has made use of the SIMBAD database, operated at CDS, Strasbourg, France (Wenger et al. 2000).

We thank the JDSO reviewer for reading this study thoroughly and thoughtfully, and for giving us many helpful and actionable comments to improve our work.

References

Bonifacio, B., C. Marchetti, R. Caputo, and K. Tock. (2020). Measurements of Neglected Double Stars. Journal of Double Star Observations, 16(5), 411–423. http://www.jdso.org/volume16/number5/Bonifacio_411_423.pdf

Doolittle, E., 1903. Mean Results of the Measures of 227 Double Stars, The Astronomical Journal, 23, 547. https://adsabs.harvard.edu/pdf/1903AJ.....23..175D

Gaia Collaboration, A. Vallenari, A. G. A. Brown, et al. (2023j) Gaia Data Release 3. Summary of the content and survey properties. A&A, 674, A1. https://arxiv.org/abs/2208.00211

Gaia Collaboration, C. Babusiaux, C. Fabricius, S. Khanna, et al. (2023) Gaia Data Release 3. Catalogue validation. A&A 674, pp. A32. https://arxiv.org/abs/2206.05989

Gaia Collaboration, T. Prusti, J.H.J. de Bruijne, et al. (2016b). The Gaia mission. A&A 595, A1. https://www.aanda.org/articles/aa/full_html/2016/11/aa29272-16/aa29272-16.html

El-Badry, K. et al. (2021) A million binaries from *Gaia* eDR3: sample selection and validation of *Gaia* parallax uncertainties. Monthly Notices of the Royal Astronomical Society, 506(2), 2269–2295. https://doi.org/10.1093/mnras/stab323

Fay, M. (2021) . El Observador de Estrellas Dobles, Issue #16, 94–96, http://www.infoastro.com/dobles/oed16.pdf

Bessell, M. S (1990). Publications of the Astronomical Society of the Pacific, 102, 1181-1199. https://adsabs.harvard.edu/full/1990PASP..102.1181B

Harshaw, Richard (2016). CCD Measurements of 141 Proper Motion Stars: The Autumn 2015 Observing Program at the Brilliant Sky Observatory, Part 3. Journal of Double Star Observations, 12(4), 394–399. http://www.jdso.org/volume12/number4/Harshaw_394_399.pdf

Morgan, S. (2023). Spectral Type Characteristics. https://sites.uni.edu/morgans/astro/course/Notes/section2/spectralmasses.html

Morgan, S. (2019). Formula - Milky Way. https://sites.uni.edu/morgans/astro/course/Notes/section3/math11.html

Bonifacio, B., C. Marchetti, R. Caputo, and K. Tock. (2020). Measurements of Neglected Double Stars. Journal of Double Star Observations, 16(5), 411–423. http://www.jdso.org/volume16/number5/Bonifacio_411_423.pdf

Wenger, M. et al. (2000). “The SIMBAD astronomical database. The CDS reference database for astronomical objects”. In: Astronomy and Astrophysics Supplement 143, pp. 9–22. DOI: 10.1051/aas: 2000332. arXiv: astro-ph/0002110 [astro-ph].

Appendix A

Table 7 contains individual astrometric measurements for each star system.

Table 7. Individual Measurements

14 images of STI 2082 (2024.0302)		10 images of POU 674 (2024.0444)		10 images of DOO 95 (2024.0329)	
Position Angle (degrees)	**Separation (arcseconds)**	**Position Angle (degrees)**	**Separation (arcseconds)**	**Position Angle (degrees)**	**Separation (arcseconds)**
359.55	6.88	27.62	8.12	172.77	8.27
359.64	6.91	27.61	8.09	172.94	8.26
359.34	6.88	27.38	8.13	172.71	8.19
359.39	6.94	27.65	8.13	172.78	8.22
359.35	7.05	27.51	8.11	172.75	8.28
359.33	6.95	27.44	8.10	172.42	8.15
359.37	6.94	27.79	8.13	173.01	8.18
359.56	6.88	27.37	8.16	172.68	8.22
359.60	6.85	27.51	8.14	172.75	8.16
359.83	6.92	27.51	8.14	173.34	8.18
359.26	7.08				
359.76	6.83				
359.43	7.06				
359.41	6.93				